Aerodynamic Optimization Using Add-On Devices: Comparison between CFD and Wind Tunnel Experimental Test

Aerodynamic optimization using add-on devices: comparison between CFD and wind tunnel experimental test

Massimiliana Carello, Marco Verratti

Abstract

JUNO is an urban concept vehicle (developed at the Politecnico of Torino), equipped by an ethanol combustion engine, designed to obtain low consumptions and reduced environmental impact. For these goals the main requirements that were considered during the designing process were mass reduction and aerodynamic optimization, at first on the shape of the car body and then, thanks to add-on devices. JUNO's aerodynamic development follows a defined workflow: geometry definition and modelling, CFD simulations and analysis, and finally geometry changes and CFD new verification. In this paper the results of the CFD simulations (using STARCCM+ and RANS k-ε) with a corresponding 1/1 scale wind tunnel tests made using the real vehicle. Particularly, the results in term of: total drag coefficient (C_x), total lift coefficient (C_z), the total pressure in the side and rear analyzing twenty different aerodynamics configurations made up of different combination of some aerodynamics add-on devices. From the analysis of the results is emerged that CFD simulations using RANS k-ε methods are able to predict the trend of total drag coefficient and its absolute value. Regarding the trend and the absolute value for lift coefficient, much larger deviation than C_x has been identified. For total pressure scene, there is a high similarity between the two ways of testing, especially on the side and on the central rear zone. The CFD results simulations, RANS k-ε model is correct to develop and test symmetrical wide body. The obtained results are in good agreement with experimental wind tunnel results but, with particular attention to geometry, that suddenly change the way of air-flow.

Introduction

Vehicle mobility is one of the most delicate and conflicting topics of the global debates of the last decades. Particularly, the problems tied to private transportation and the relationship between citizens, cars and cities are seeing developments that would have been unthinkable a few years ago. Atmospheric and acoustic pollution, the congestion and degradation of urban areas (caused by the physical space occupied by cars) and the exploitation of ground space (caused by the construction of streets and infrastructure) are just some of the many problems tightly connected to vehicles. Large automobile manufacturers are working hard to realize prototypes of eco-friendly cars that use hydrogen, bio-fuels, pressurized natural gas or electricity as sources of energy to find real alternatives to oil.

The Shell Eco Marathon is born in this scenario of the pursuit of innovative solutions to transportation, aimed at a reduction of fuel consumption and pollutant emissions. It's addressed to student teams from all over the world, who plan, build, and field highly energy-efficient vehicles. This initiative is a stimulating challenge for the thousands of participants and spectators, who get to apply concrete thought to the current and future problems of transportation and energy, spearheading innovative solutions to improve sustainable mobility. Although the rules of the competition impose strict project limitations, they give free rein on defining the vehicle's shape and on choosing the energy source from the available options (gasoline, diesel, alcohol, hydrogen, solar, electric, etc...).

JUNO, designed at Politecnico of Torino, (Figure 1) is a prototype of urban vehicle supplied by bioethanol. The goal is to participate in the European Shell Eco Marathon, a competition where the winner is, for each category, the vehicle, which obtains the lowest fuel consumption during the competition. This means getting a higher km/L value. JUNO is an urban vehicle intended to have low consumption and reduced environmental

impact. The design process was followed in absolute compliance with the strict rules that Shell imposes to participate in its competitions, keeping an eye on the needs of the automobile market, which is going through deep and sustained changes [1, 2].

JUNO is the vehicle considered as a case study for all the CFD analyses, experimental wind tunnel tests and comparisons found in this paper.

Figure 1 The Urban concept JUNO

The vehicle JUNO and the wind tunnel

Full scale experimental tests were undertaken at the Stellantis research center in Orbassano (TO) inside a closed-circuit subsonic wind gallery (the flow is put back into circulation using a single return duct [3]). The main reference characteristics used to recreate the virtual environment are the size of the testing tunnel are: 10.5 m length, 12 m width, 12 m height, reference values of Turbulence Length scale equal to 0.001 m and Turbulence Intensity equal to 0.005.

The vehicle dimensions are reported in Table 1. To fix it inside the wind tunnel (designed for commercial cars) without damaging the moving ground mechanism some adjustments have been done and transversal brackets have been placed under the vehicle and covered with NACA 0015 air foils with the aim of reducing any disturbance they might cause (Figure 2).

Table 1 JUNO's dimensions

	JUNO dimension
Length	2.88 m
Height	1.17 m
Wheelbase	1.6 m
Track	1.0 m
Frontal Area	1.2 m^2

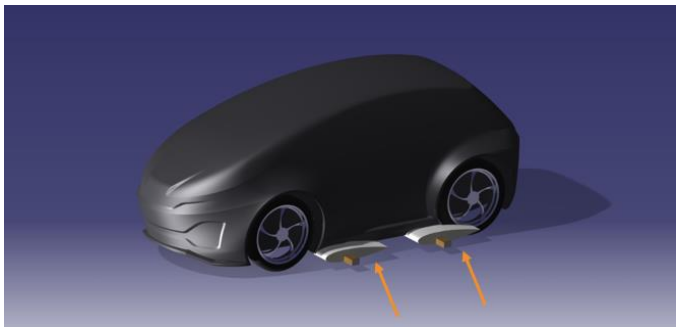

Figure 2 JUNO and airfoils

For the execution of the experimental tests a low-roughness film was applied to the NACA foils to minimize the effect of viscous friction and another modification was made specifically for the wheels, to guarantee their rotation and ensure contact with the mobile floor a concentric strip of rubber around them has been placed, to increase the tire width (Figure 3).

Figure 3 Rubber circumferences around JUNO's tyres

Computational Fluid Dynamics settings

The virtual simulation environment was built based on the real wind gallery, but with an increase in size to minimize the boundary effects. Here is a representative image of the virtual gallery (Figure 4). Three elements have particular importance:

- the stationary floor (in pink), which thanks to the slip condition simulates the boundary layer present in a real tunnel;

- the mobile ground (in gray);

- the symmetry plane (in blue), that corresponds to the geometric symmetry of the vehicle, has been chosen to have lower computational cost (and so a lower calculation time), with an acceptable resolution [4].

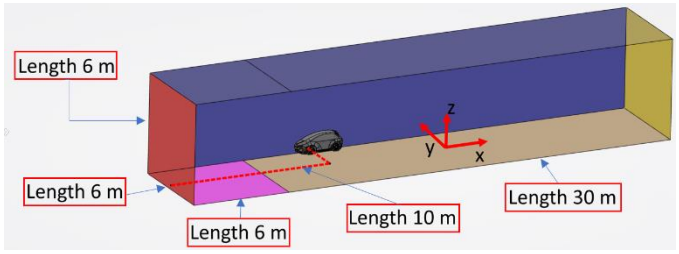

Figure 4 Virtual wind tunnel dimensions

For the validation stage of the numerical method, the fully turbulent RKE 2L method (k-ε Two-Layer), has been selected. This method, whose transport equations for kinetic energy (Equation 1) [5] and for turbulent dissipation rate (Equation 2) [5], makes use of the RANS (Raynolds-Avereged Navier-Stokes), but applies a minimum limit on the turbulence's temporal scale to prevent the large increase in turbulent kinetic energy

(common in two-equation models) from interfering critically with the overall result. The choice of this method gives the best compromise between computational cost and accuracy of the results if the wall effects are not as relevant as those in the wake [6].

$$\frac{\partial}{\partial t}\left(\rho k\right)+\nabla\cdot\left(\rho k\bar{\mathbf{v}}\right)=\nabla\cdot\left[\left(\mu+\frac{\mu_t}{\sigma_k}\right)\nabla k\right]+P_k-\rho(\varepsilon-\varepsilon_0)+S_k \quad (1)$$

$$\frac{\partial}{\partial t}\left(\rho\varepsilon\right)+\nabla\cdot\left(\rho\varepsilon\bar{\mathbf{v}}\right)=\nabla\cdot\left[\left(\mu+\frac{\mu_t}{\sigma_\varepsilon}\right)\nabla\varepsilon\right]+\ldots$$

$$+\frac{1}{T_e}C_{\varepsilon 1}P_\varepsilon-C_{\varepsilon 2}f_2\rho\left(\frac{\varepsilon}{T_e}-\frac{\varepsilon_0}{T_0}\right)+S_\varepsilon \quad (2)$$

Regarding the initial conditions set in the simulation, the parameters given by the wind gallery as pertaining to the turbulence length scale and turbulence length intensity have been used, while to set the turbulence velocity scale at 70 km/h since it is the simulation's representative speed, as well the entry speed of the undisturbed flow have been defined.

Regarding the creation of the computational domain, to use a polygonal-type grid with the knowledge that such elements are more computationally costly, but at the same time offer, a greater resolution has been chosen. During the process of defining the mesh, the density of certain areas around the vehicle, without limiting ourselves to the typical areas of interest, have been carefully increased, instead concentrating also on the areas where the appendages used in the test will be mounted (Figure 5). This choice is supported by a grid independence study that showed an asymptotic tendency of the solution over 4.5 MLN of cells.

During this phase the fundamental aspects to keep in consideration are the definition of the boundary layer and the value of the Y+ [1] parameter for the whole vehicle. As a result of the settings that have used a mesh containing: 4.625.070 cells, 23.873.029 faces and 16.811.662 vertices. These grid cells demonstrate a high quality (Figure 6 and Figure 7), with the exception of 11, which were distant from the vehicle, and thus we decided to remove them from the computational domain.

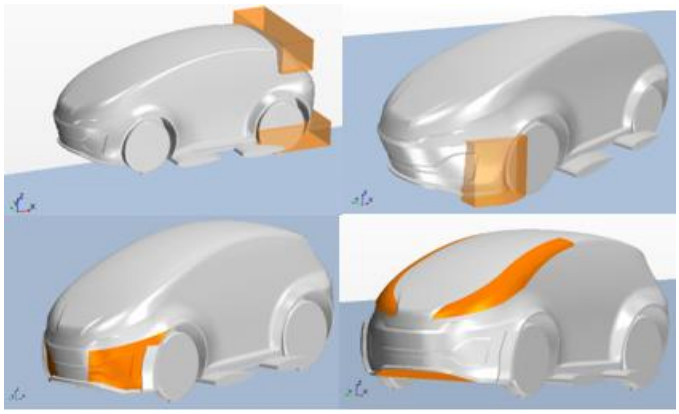

Figure 5 Volume and surface control for mesh refinement near add-on devices (orange)

[1] Y+ is a parameter that identifies the sublayer that houses a single cell. There are 3 intervals, which define as many sublayers: Y+< 5 laminar, Y+> 30 turbulent, 5< Y+ < 30 transitional.

```
-> FACE VALIDITY STATISTICS:
Minimum Face Validity: 1.000000e+00
Maximum Face Validity: 1.000000e+00
         Face Validity <  0.50            0     0.000%
0.50 <= Face Validity <  0.60            0     0.000%
0.60 <= Face Validity <  0.70            0     0.000%
0.70 <= Face Validity <  0.80            0     0.000%
0.80 <= Face Validity <  0.90            0     0.000%
0.90 <= Face Validity <  0.95            0     0.000%
0.95 <= Face Validity <  1.00            0     0.000%
1.00 <= Face Validity              4625070   100.000%
```

Figure 6 Mesh quality, face validity

```
-> VOLUME CHANGE STATISTICS:
Minimum Volume Change: 3.730953e-03
Maximum Volume Change: 1.000000e+00
         Volume Change <  0.000000e+00           0    0.000%
0.000000e+00 <= Volume Change <  1.000000e-06           0    0.000%
1.000000e-06 <= Volume Change <  1.000000e-05           0    0.000%
1.000000e-05 <= Volume Change <  1.000000e-04           0    0.000%
1.000000e-04 <= Volume Change <  1.000000e-03           0    0.000%
1.000000e-03 <= Volume Change <  1.000000e-02          11    0.000%
1.000000e-02 <= Volume Change <  1.000000e-01       45838    0.991%
1.000000e-01 <= Volume Change <= 1.000000e+00     4579221   99.009%
```

Figure 7 Mesh quality, volume change

CFD and wind tunnel testing comparison

The entire study concerns CFD simulations and experimental wind gallery tests. The comparison of the following configurations (if not specified the test is done with lenticular wheels and a speed of 70 km/h):

1) standard configuration -70 km/h (devoid of all add-on devices).

2) standard configuration – 60 km/h (devoid of all add-on devices).

3) standard configuration – 50 km/h (devoid of all add-on devices).

4) front C + spoiler 0° + rear diffusor 7° + air dam + finlet 2 + telemetry

5) front C + spoiler 0° + air dam + finlet 2

6) front C + spoiler 0° + air dam + finlet 1

7) front C + spoiler 0° + air dam

8) spoiler 0° + air dam

9) spoiler 7° + rear diffuser 0° + air dam

10) spoiler 7° + rear diffusor 0°

11) spoiler 0°

12) spoiler 7°

13) spoiler -7°

14) standard ¬ yaw angle 2°

15) standard ¬ yaw angle 5°

16) standard ¬ yaw angle 10°

17) telemetry

18) front C (without lenticular wheels)

19) complete configuration with front C + spoiler 0 ° + rear diffuser 7 ° + air dam + finlet 2, without lenticular wheels (represented from Figure 8 to Figure 12).

Specifically, in this paper the results of the two configurations 1) and 19) (more representative) are presented.

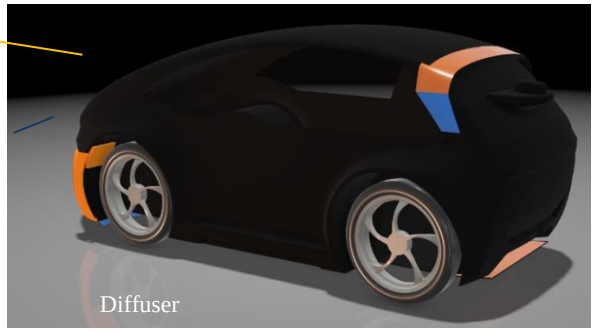

Figure 8 JUNO's aero pack in orange and blue

Figure 9 JUNO's Diffuser position

a)

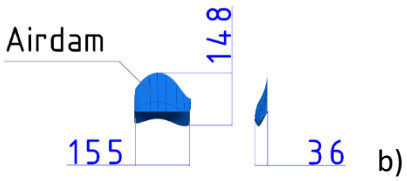

b)

Figure 10 JUNO's Air dam: a) position, b) dimensions

a)

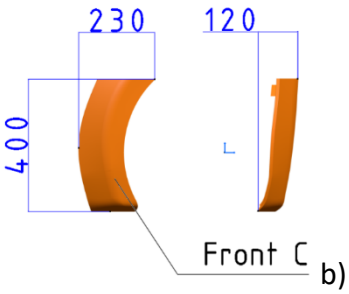

b)

Figure 11 JUNO's Front C: a) position, b) dimensions

a)

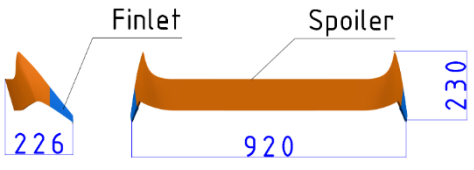

b)

Figure 12 JUNO's Spoiler and Finlet: a) position, b) dimensions

The parameters considered for this comparison are:

- Drag coefficient (C_x),
- Lift coefficient (C_z),
- Total Pressure.

From Figure 13 to Figure 18 report the results of the complete configuration first, then of the standard configuration, representing the stabilization of the results and their asymptotic convergence. In particular the CFD results has been obtained using the k-ε turbulence model, that it has been modified in a second step, changing and adopting the k-ω turbulence model, more suitable to evaluate the boundary effects. For this reason, the influence of turbulent model is greater on the C_x than on C_z.

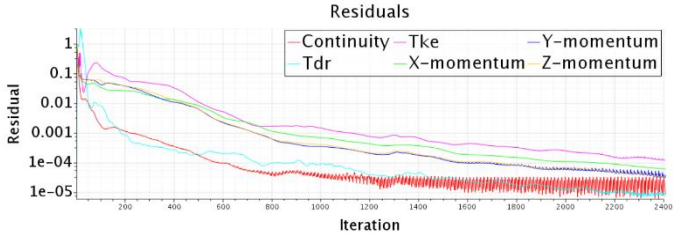

Figure 13 Complete configuration, residuals trend normalized to the value of 0.1

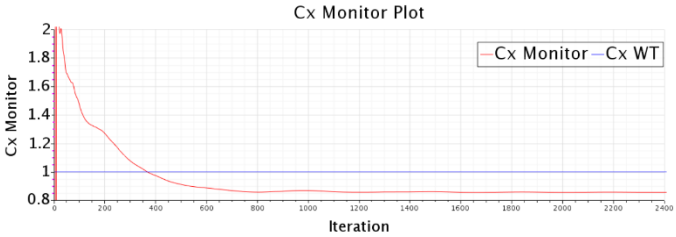

Figure 14 Complete configuration, C_x trend normalized to wind tunnel value

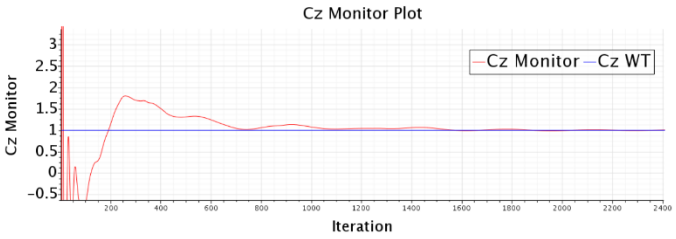

Figure 15 Complete configuration, C^z trend normalized to wind tunnel value

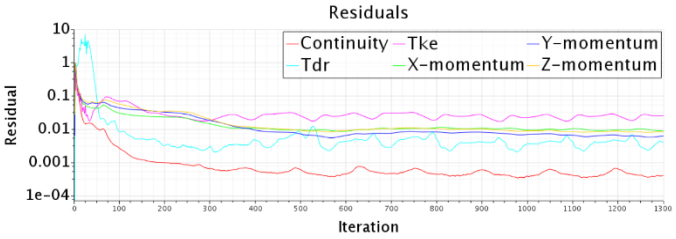

Figure 16 Standard configuration, residuals trend normalized to the value of 0.1

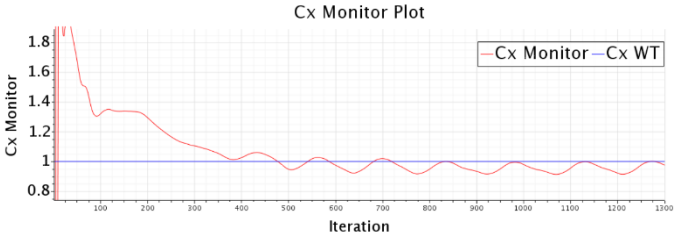

Figure 17 Standard configuration. C_x trend normalized to wind tunnel value

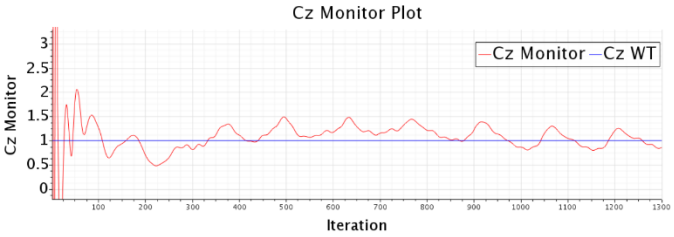

Figure 18 Standard configuration, C_z trend normalized to wind tunnel value

In numerical terms, the two configurations (complete and standard) give notably different uncertainty levels when applied to the experimental tests. As can be noted in Table 2, the complete configuration reports an differential relative to C_x that is about 14% relative to the experimental tests, indicating an underestimation of its value. As far as the C_z value is concerned though, this configuration is the only one out of all those tested to have a lift coefficient without oscillations, thus obtaining a result almost identical to the experimental one. Regarding the standard configuration, it is possible to see in Table 2 that the uncertainty relative to C_x is less than 1%, ranging from 0.1% and 0.9%, while C_z has a wider oscillation, which brings it to have an uncertainty somewhere between 15% and 20%.

Regarding the comparison in terms of total pressure, it has been acquired, during the wind tunnel tests, using various pitot tubes set in motion to cover the areas represented in Figure 19 and Figure 20.

Table 2 Numerical comparison between CFD and wind tunnel for Complete and Standard configuration

	Standard Configuration	Complete configuration
C_x Wind Tunnel	0.407	0.354
C_x CFD	0.403	0.310
Δerr	0.4 %	14 %
C_z Wind Tunnel	0.095	0.095
C_z CFD	0.109	0.096
Δerr	15 %	0.1 %

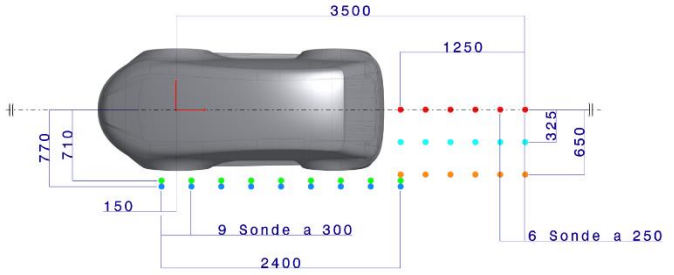

Figure 19 JUNO and pitot probe, top view

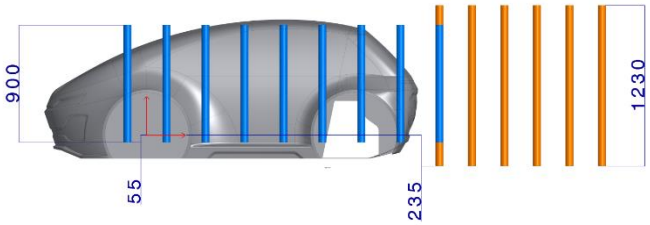

Figure 20 JUNO and pitot probe, side view

Thanks to a Matlab script (developed specifically for this study) has been imported the total pressure values measured from those same points and represented them in 3D graphs to facilitate their study. The graphs (Figure 21 and Figure 22), show the complete configuration's rear wake for the wind tunnel and the simulation. Figure 23 and Figure 24 show the complete configuration's lateral wake for the wind tunnel and the simulation. From Figure 25 to Figure 28 rear and lateral wake in both conditions are shown.

Figure 21 and Figure 22 indicate a tight correlation between the wind gallery tests and the CFD ones: in fact, it is possible to see that the wake's trend is almost the same and the total pressure's error is around 0.4%. The most marked differences are, on the plane that divides the vehicle longitudinally (y=0), in the wake's entrance, where we can notice a first part of the wake which is tighter in the simulations than in the experimental tests. On the other planes, the two trends are qualitatively identical.

Regarding the lateral part of the vehicle, comparing Figure 23 and Figure 24 a strong similarity between the wakes are highlight. In fact, even in this case the deviation between the CFD and experimental results is essentially equal to zero.

The standard configuration is very similar to the complete configuration as far as the rear wake is concerned. By observing Figure 25 and Figure 26 the negative Y planes have identical trends in both trials (CFD and wind gallery), which is not the case on the Y = 0 plane where, especially in the lower part, closer to the vehicle, there is a small deviation. Also in the standard configuration, the wake in the CFD simulations closes earlier than the one observed in the wind tunnel.

Regarding the total pressure in the lateral part of the vehicle a slightly lower accuracy compared to that of the complete configuration is point out. By observing Figure 27 and Figure 28 it is possible to see how in this test a slight deviation is noticeable especially in the probes placed at Y = -0.71 where in the simulation, the wake tends to close and then widen back again, a phenomenon not observed in the wind tunnel.

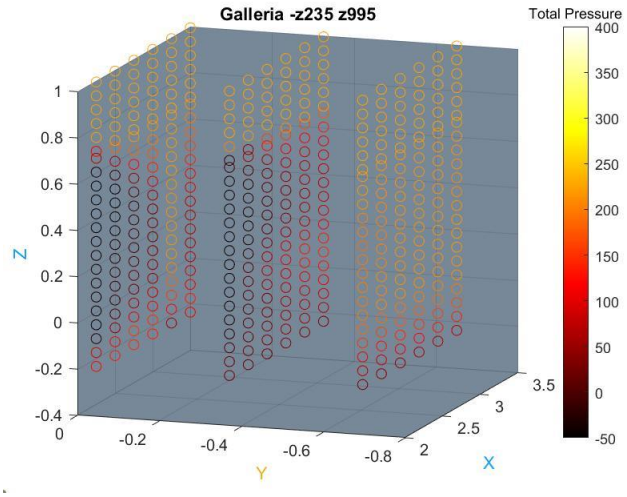

Figure 21 Complete configuration, rear wake wind tunnel value

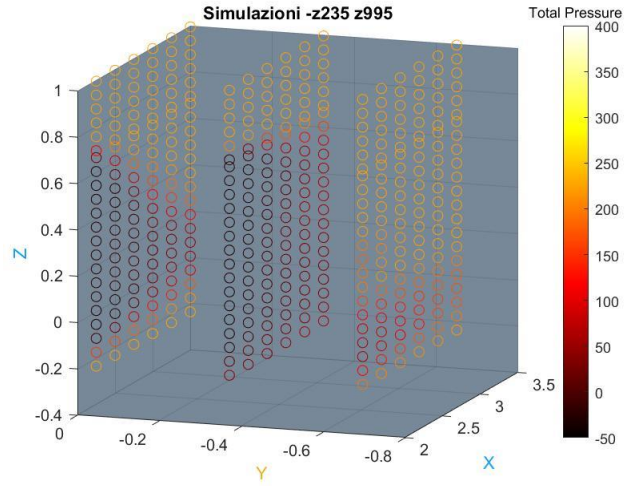

Figure 22 Complete configuration, rear wake CFD value

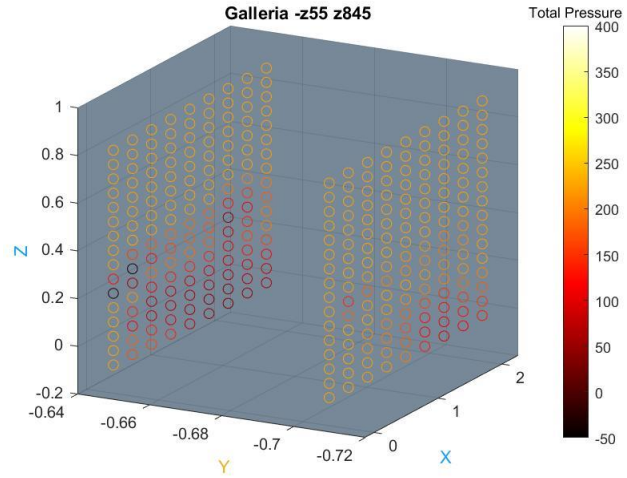

Figure 23 Complete configuration, side wake wind tunnel value

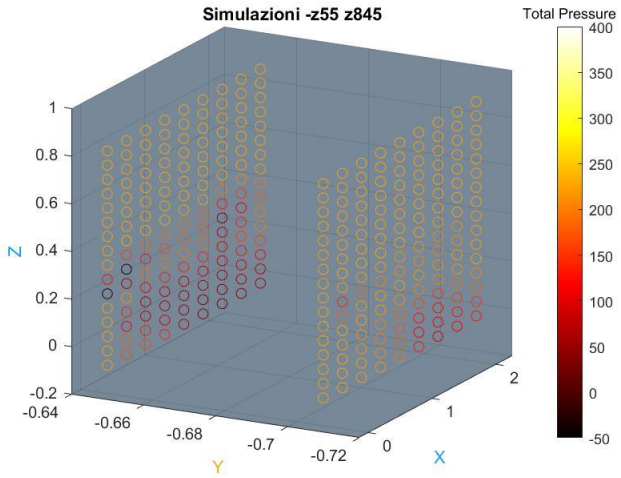

Figure 24 Complete configuration, side wake CFD value

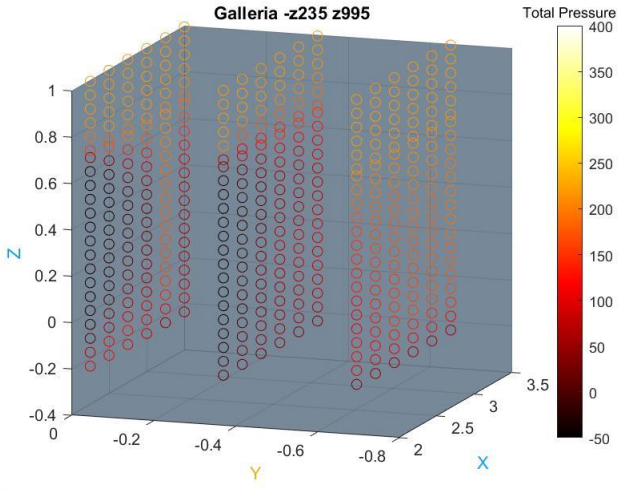

Figure 25 Standard configuration, rear wake wind tunnel value

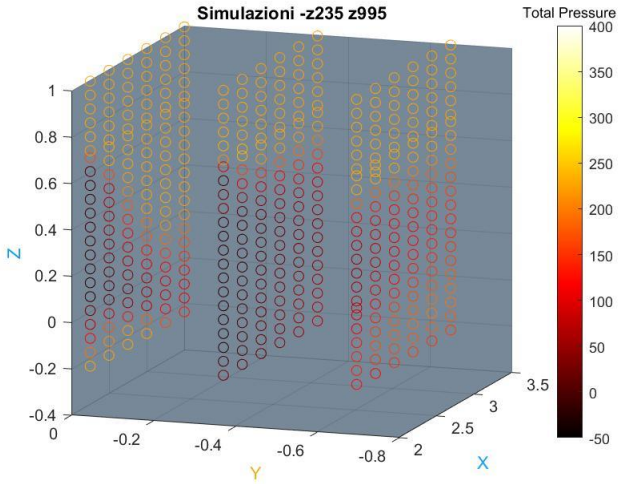

Figure 26 Standard configuration, rear wake CFD value

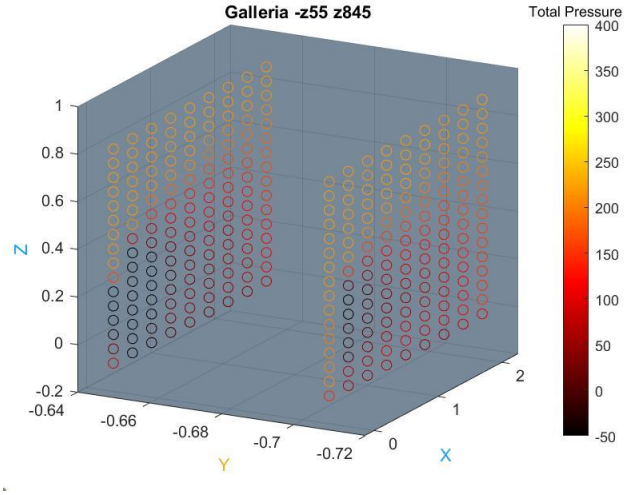

Figure 27 Standard configuration, side wake wind tunnel value

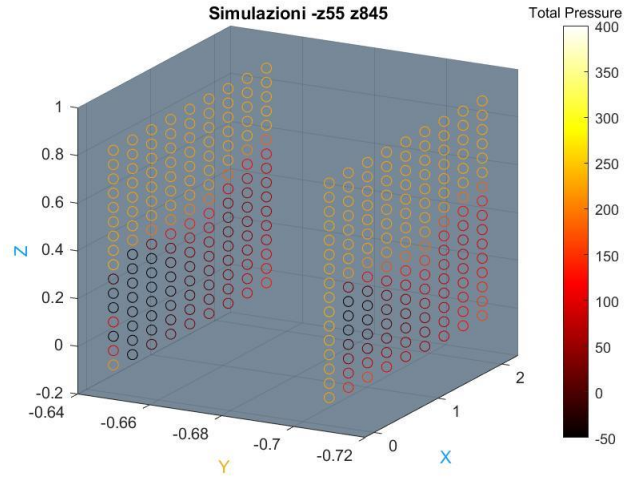

Figure 28 Standard configuration, side wake wind CFD value

By observing from Figure 29 to Figure 32, what emerged from the comparison of the trends of total pressure becomes clear. The numerical simulations show a much more definite narrowing of the wake than the one that emerged from the experimental tests. This result is probably due to the initially chosen numerical model, which, resolving the field of motion in the wake of the vehicle more accurately, gives results close to the experimental ones, but loses resolution where higher precision is required, as in the cells near the walls. This may also be effected by the longitudinal static pressure gradient present in the wind tunnel, which would not be present in your simulation unless you simulated the nozzle, plenum chamber, collector and diffuser sections.

Figure 29 Complete configuration, JUNO's smoke wind tunnel test

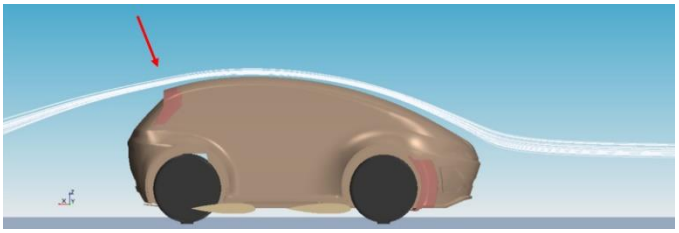

Figure 30 Complete configuration, JUNO streamlines scene CFD

Figure 31 Standard configuration, JUNO's smoke wind tunnel test

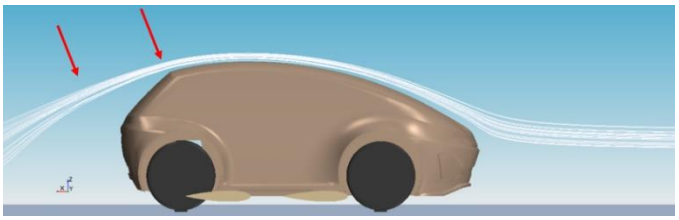

Figure 32 Standard configuration, JUNO's CFD streamlines scene

Turbulence model comparison

The last part of the paper regards to the comparison of two other numerical simulation methods, in particular:

- SST k-ω model;

- Gamma ReTheta Transition Model.

The two models were used for the complete configuration only because it ends up being the one with an uncertainty level over the 10% threshold.

The SST k-ω model was chosen for its quality of being a combination of the k-ε and k-ω models. In this way, by implementing a switch between the two models, it is excellent in solving both the field of motion close to the wall and the one in the wake, at the price of a sharp increase in computational cost. The equations for the transportation of kinetic energy K (Equation 3) and the specific dissipation rate W (Equation 4) are shown reported.

$$\frac{\partial}{\partial t}(\rho k) + \nabla\cdot(\rho k\bar{\mathbf{v}}) = \nabla\cdot\left[\left(\mu + \sigma_k\mu_t\right)\nabla k\right] + P_k - \rho\beta^* f_{\beta^*}\left(\omega k - \omega_0 k_0\right) + S_k \quad (3)$$

$$\frac{\partial}{\partial t}(\rho\omega) + \nabla\cdot(\rho\omega\bar{\mathbf{v}}) = \nabla\cdot\left[\left(\left(\mu + \sigma_\omega\mu_t\right)\nabla\omega\right] + P_\omega - \rho\beta f_\beta\left(\omega^2 - \omega_0^2\right) + S_\omega \quad (4)$$

A necessary modification for the use of this numerical method was executed on the mesh's prism layer since

the optimal use of the SST k-ω model requires a Y + value close to 1. For this reason, the number of prism layers around the vehicle has been increased, thus also increasing its total thickness. Once reached a stable numerical result (Figure 33) and thus a convergence with the physical result (Figure 34 and Figure 35), the results have been analyzed and found a marked improvement of C_x compared to the simulation executed with the k-ε method.

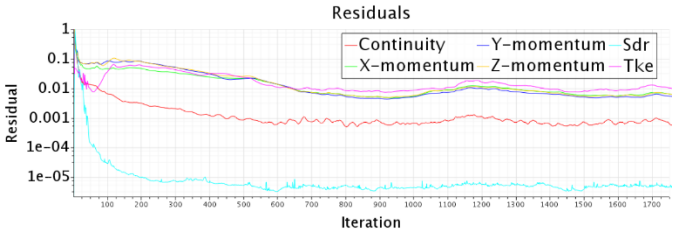

Figure 33 Complete configuration, residuals trend normalized to the value of 0.1, SST k-ω

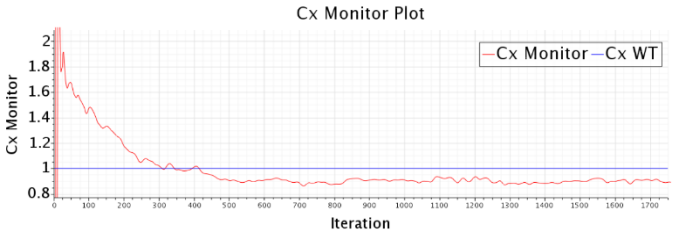

Figure 34 Complete configuration, C_x trend normalized to wind tunnel value, SST k-ω

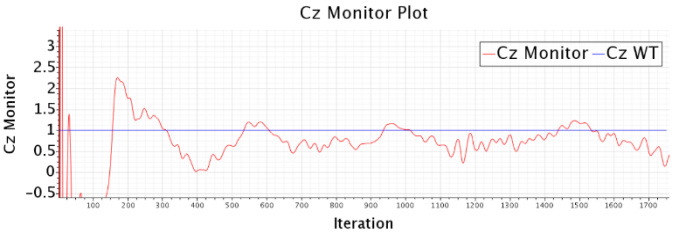

Figure 35 Complete configuration, C_z trend normalized to wind tunnel value, SST k-ω

However, Cz registers a worsening of the stability of its results. In fact, a fluctuation in the trend, which was not present with the previous method have been registered. Table 3 shows the comparison between the SST K-W model's results and those acquired during the wind gallery tests.

Table 3 Numerical comparison between CFD and wind tunnel, SST k-ω

	Complete configuration
C_x Wind Tunnel	0.354
C_x CFD	0.320
Δerr	9.6 %
C_z Wind Tunnel	0.095
C_z CFD	0.075
Δerr	21 %

As for the flow trend in the wake of the vehicle, as can be observed in Figure 36, no clear differences were noted between the use of the k-ε model (Figure 30) and the and k-ω one.

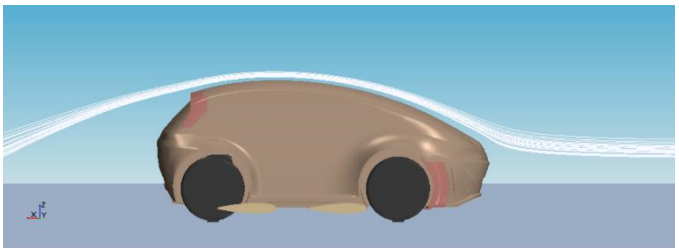

Figure 36 Complete configuration, JUNO streamlines scene CFD and SST k-ω model

Regarding the SST k-ω model with Gamma Re Theta transition, it has chosen a transition model to better evaluate the flow's transition from laminar to turbulent, thus obtaining a value closer to the actual momentum in the boundary layer and observing the detachment of the fluid vein with less uncertainty. In this model, Equations 3 and 4, two more transport equations, one for the γ intermittence (Equation 5) and one for the transition momentum thickness Reynolds number (Equation 6) $Re_{\theta t}$ have been added.

$$\frac{d}{dt}(\rho\gamma) + \nabla\cdot\rho\gamma\bar{\mathbf{v}} = \nabla\cdot\left[\left(\mu + \frac{\mu_t}{\sigma_f}\right)\nabla\gamma\right] + P_\gamma - E_\gamma \quad (5)$$

$$\frac{d}{dt}(\rho\overline{Re_{\theta t}}) + \nabla\cdot(\rho\overline{Re_{\theta t}}\bar{\mathbf{v}}) = \nabla\cdot\left[\sigma_{\theta t}(\mu + \mu_t)\nabla\overline{Re_{\theta t}}\right] + P_{\theta t} + D_{SCF} \quad (6)$$

Again, it is necessary to modify the grid, as for the optimal use of this model it's advised to have a value of Y+ ≤ 1. For this reason, has been chosen to further increase the number of wall layers around the vehicle, slightly increasing the thickness value of the boundary layer. In addition, to use this model we need to supply a function that allows the method to discern between when to consider the free stream situation and when to consider the one inside the boundary layer. For this reason, a simple function, shown in Equation 7 (where ? represent an "if" function), has been implemented inside the simulation software. This turbulence model consider a free stream for values, which are outside a certain distance from the wall, and while values inside should be considered as a boundary layer.

$$\$\boldsymbol{WallDistance} > \mathbf{0.04}?\,\mathbf{1}:\mathbf{0} \quad (7)$$

The value 0.04 was calculated assuming a fully turbulent boundary layer, obtaining a value of about $3.79\cdot10^{-2}$ m using Equation 8.

$$\delta = 0.37 \cdot L \cdot \left(\frac{1}{Re}\right)^{\frac{1}{5}} \quad (8)$$

This simulation resulted in better stability than the SST k-ω case, as can be seen from Figure 37 to Figure 39.

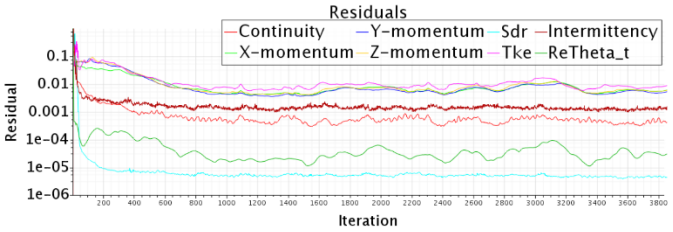

Figure 37 Complete configuration, residuals trend normalized to the value of 0.1, SST k-ω Gamma ReTheta

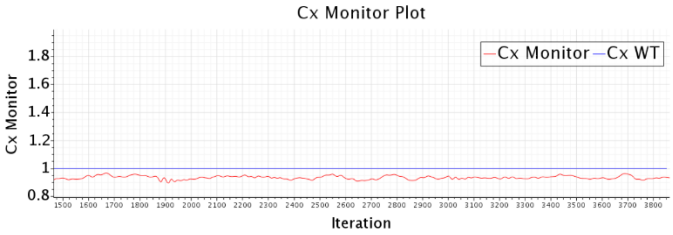

Figure 38 Complete configuration, Cx trend normalized to wind tunnel value, SST k-ω Gamma ReTheta

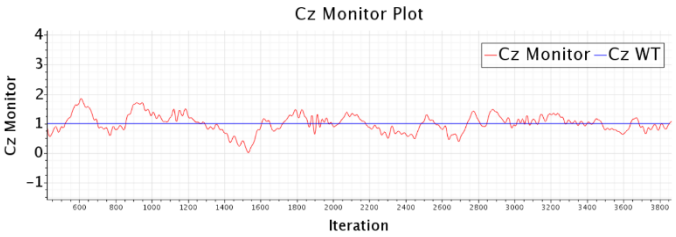

Figure 39 Complete configuration, Cz trend normalized to wind tunnel value, SST k-ω Gamma ReTheta

As far as C_x is concerned, a slight convergence of the simulated values to the experimental ones has been observed. The results of Table 4 point out that the uncertainty is lower than in the SST k-ω model. This improvement of C_x does not impact C_z's stability, as can be seen in Figure 39. In fact, in this case, we can notice a sharp improvement in C_z's stability, which positively affects the uncertainty level, as observable in Table 4.

Table 4 Numerical comparison between CFD and wind tunnel, SST k-ω Gamma ReTheta

	Complete configuration
Cx Wind Tunnel	0.354
Cx CFD	0.336
Δerr	5.1 %
Cz Wind Tunnel	0.095
Cz CFD	0.085
Δerr	10 %

By observing the scene's streamlines (Figure 40) and comparing them with Figure 30, no large differences in qualitative terms have been observed. This is probably due to a non-optimal choice of the parameters that determine the correction of the streamlines' curvature; the parameters influence the curves in accordance with the physical results.

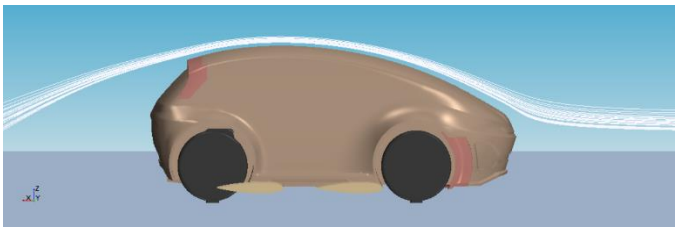

Figure 40 Complete configuration, JUNO streamlines scene CFD, SST k-ω Gamma ReTheta

Conclusion

This paper started from previous studies regarding “a small vehicle” and the use of the add-on devices to improve the aerodynamic performance and reduce the vehicle energy consumption [8-10].

In particular, this paper presents a CFD model and experimental validation for a small vehicle JUNO, adapting the connection and use of the wind tunnel, evaluating the influence of different turbulence models and considering the vehicle in different configurations (using different add-on devices to increase the efficiency).

It’s evident how the k-ε turbulence model is more appropriate when analyzing a field of motion around an object where the wake component is more important than the boundary layer. In fact, it is possible to deduce that the configurations considered (Table 3) reach uncertainty levels for C_x, which are noticeably lower than 10%. This threshold is regarded in the literature as acceptable to validate a numerical test in relation to an experimental wind tunnel one [7]. In those situations where the fluid vein is noticeably detached, and so the wall flow is particularly important, the k-ε model give elevated levels of uncertainty. On the contrary, the SST k-ω model (or in particular the SST k-ω combined with the Gamma ReTheta transition) predicts the wall flow better, thus reducing the uncertainty between the numerical tests and the experimental tests.

For a better comparison, all of the spoilers have been tested with all the turbulence model studied in this paper. Results shown from Figure 41 to Figure 43 confirm all the test done.

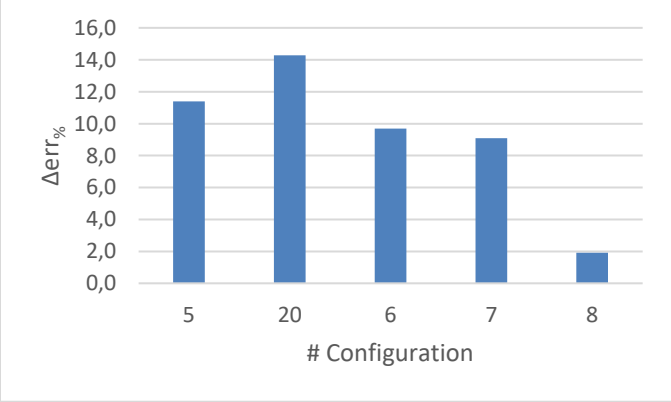

Figure 41 Spoiler's included configuration k-ε

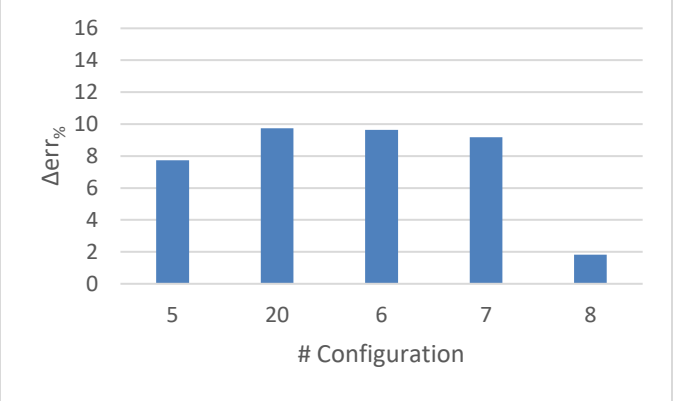

Figure 42 Spoiler's included configuration k-ω SST

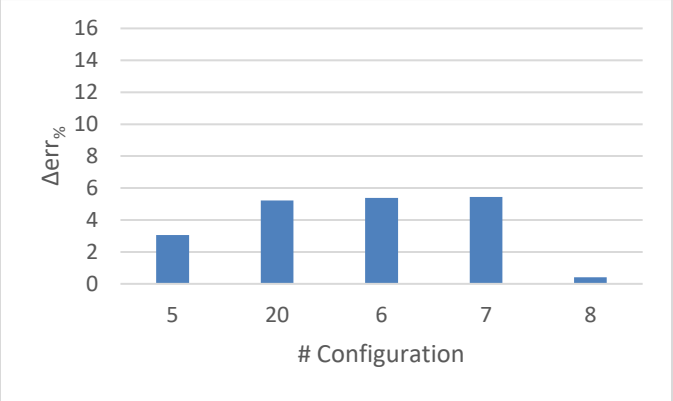

Figure 43 Spoiler's included configuration k-ω SST Gamma Re Theta

References

1. M. Carello, “Innovative and multidisciplinary teaching through the design and construction of low consumption vehicles for international competitions”, 2nd International Symposium on the Education in Mechanism and Machine Science, Mechanisms and Machine Science - New trend in Educational Activity in the Field of Mechanism and Machine Theory, Springer, pp. 8, Vol. 64, 2019, ISBN: 978-3-030-00107-0, doi: 10.1007/978-3-030-00108-7_9.
2. M. Carello, “Innovative and Multidisciplinary Teaching to Design a Low Consumption Vehicle”, International Workshop IFToMM for Sustainable Development Goals, I4SDG Workshop 2021, Mechanisms and Machine Science, pp. 641–650, vol 108, Springer, doi: 10.1007/978-3-030-87383-7_69.
3. Polezhaev Y. V. , “Wind Tunnel”, Thermopedia technical paper 2011-02-02, doi: 10.1615/AtoZ.w.wind_tunnels
4. Melber-Wilkending S., Heidebrecht A. and Wichmann G., “CFD validation by wind tunnel measurement”, STO NATO technical paper RTO-TR-027, doi: 10.14339/RTO-TR-027.
5. Siemens PLM Software, “STAR-CCM+® Documentation Version 13.02, Siemens, 2018”.
6. Campanini L., “Corpo di calibrazione: confronto al CFD fra configurazioni di flusso libero e flusso in galleria del vento”, master thesis available on core.ac.uk numero: 14698633.
7. Moonena P., Blockena B., Roelsa S. and Carmeliet J., “Numerical modeling of the flow conditions in a closed-circuit low-speed wind tunnel”, doi: 10.1016/j.jweia.2006.02.001.
8. Carello M., Serra A., Airale A.G., Ferraris A., “Design the City Vehicle XAM using CFD Analysis”, SAE World Congress, Detroit – USA, 21-23 April 2015, pp. 7, doi: 10.4271/2015-01-1533.
9. Ferraris A., Airale A.G., Berti Polato D., Messana A., Xu S., Massai P., Carello M., “City Car Drag Reduction by Means of Shape Optimization and Add-On Devices”, Mechanisms and Machine Science, Springer

Netherlands, pp. 10, Vol. 73, 2019, ISSN: 2211-0984, ISBN: 978-3-030-20130-2, doi: 10.1007/978-3-030-20131-9_367.
10. Ferraris, A.; de Carvalho Pinheiro, H.; Airale, A. G.; Carello, M.; Berti Polato, D., "City Car Drag Reduction by means of Flow Control Devices", SAE Technical Paper, 2020 SAE Brasil Congress and Exhibition, Sao Paulo (Brasil), pp. 9, 2021, Vol. 1, ISSN: 0148-7191, DOI: 10.4271/2020-36-0080.

Contact Information

Massimiliana Carello

Politecnico di Torino - Mechanical and Aerospace

Engineering Department

Corso Duca degli Abruzzi, 24; 10129 Torino - Italy

massimiliana.carello@polito.it

Acknowledgments

Thanks to the remaining part of the Team H_2politO that made possible the realization of this project and in particular to the aerodynamic group (Matteo Savi, Danilo Caterino and other) for the help and simulation activity year by year.

Thanks to Siemens for providing software simulation tools and Stellantis Group for the wind tunnel availability, in particular Marco Stellato and Gianni Sampaolo for the help during the test.

The vehicle JUNO is financially supported by the "Committee on Contributions and funds for students projects" of the Politecnico of Turin and other sponsors and technical partners (see also www.polito.it/h2polito).

Definitions/Abbreviations

WT – Wind tunnel

CFD – Computational Fluid Dynamics

C_x – Drag force coefficient

C_z – Lift force coefficient (+) or Down force coefficient (-)

Δerr – Delta error between two quantities

Airdam – Add on devices placed on the vehicle floor after front wheels

ρ - Air density

k – Kinetic energy

ε – Turbulent dissipation rate

ω – Specific dissipation rate

$\varepsilon_0,\ \omega_0, \mathrm{k}_0$ – Turbulent dissipation rate, Specific dissipation rate and Kinetic energy at ambient conditions

$\overline{\mathrm{V}}$ – Mean velocity

μ – Dynamic viscosity

μ_t – Turbulent eddy viscosity

β – Thermal expansion coefficient

$\sigma_\mathrm{k}, \sigma_\varepsilon, \sigma_\omega, \sigma_\mathrm{f}, \sigma_{\theta\mathrm{t}}, \mathrm{C}_{\varepsilon 1}, \mathrm{C}_{\varepsilon 2}, \beta^*$ – Model coefficients

$\mathrm{P}_\mathrm{k}, \mathrm{P}_\varepsilon, \mathrm{P}_\omega, \mathrm{P}_\gamma, \mathrm{P}_{\theta\mathrm{t}}$ – Production terms

E_γ – Destruction term

$\mathrm{D}_{\mathrm{SCF}}$ – Cross-flow term

f_2 – Damping function (mimic the decrease of turbulent mixing near the walls)

f_{β^*} - Free-shear modification factor

f_β – Vortex-stretching modification factor

$\mathrm{S}_\mathrm{k}, \mathrm{S}_\varepsilon, \mathrm{S}_\omega$ – User-specified source terms

T_e – Large-eddy time scale

T_0 – Specific time-scale

γ – Intermittency

$\overline{\mathrm{Re}_{\theta\mathrm{t}}}$ – Transition momentum thickness Reynolds number